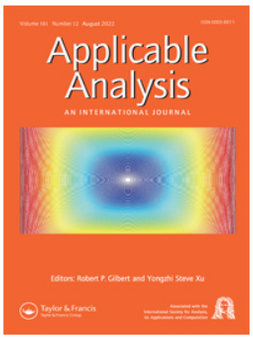

Taylor & Francis
Taylor & Francis Group

Applicable Analysis

An International Journal

ISSN: (Print) (Online) Journal homepage: https://www.tandfonline.com/loi/gapa20

Space-time geometric multigrid method for nonlinear advection–diffusion problems

Hanyu Li & Mary F. Wheeler

To cite this article: Hanyu Li & Mary F. Wheeler (2022) Space-time geometric multigrid method for nonlinear advection–diffusion problems, Applicable Analysis, 101:12, 4194-4202, DOI: 10.1080/00036811.2022.2039387

To link to this article: https://doi.org/10.1080/00036811.2022.2039387

Published online: 13 Feb 2022.

APPLICABLE ANALYSIS
2022, VOL. 101, NO. 12, 4194–4202
https://doi.org/10.1080/00036811.2022.2039387

Taylor & Francis
Taylor & Francis Group

Space-time geometric multigrid method for nonlinear advection–diffusion problems

Hanyu Li and Mary F. Wheeler

Oden Institute for Computational Engineering and Sciences, Austin, TX, USA

ABSTRACT

Multigrid methods, algebraic or geometric, commonly suffer from high frequency residuals after prolongation. This paper develops a stable approach to remove high frequency residuals for geometric multigrid methods for solving nonlinear advection–diffusion problems with degenerate coefficients. Here, a local problem is treated by optimization on subdomains with mesh refinements. Newton's method is utilized in the procedure and the iteration is completed when the residual in the subdomain is reduced to the given magnitude, usually set to be the average of residuals in the non-high-frequency domains. An oversampling technique is employed to further improve the stability by providing a definite flow path in regions where coefficients have high contrast and complex structures. Removing high frequency residuals before continuing the global Newton iteration improves global convergence behavior.

ARTICLE HISTORY
Received 17 October 2021
Accepted 2 February 2022

COMMUNICATED BY
G. Allaire

KEYWORDS
Local residual minimization; smoothing; geometric multigrid; advection–diffusion problem; mixed finite element method

2020 MATHEMATICS SUBJECT CLASSIFICATIONS
35D30; 86-08; 86-10; 65M55; 65M60

1. Introduction

Models describing complex phenomena involving multiple physical processes are often computationally prohibitive, due to significant nonlinearities and problem size. The geometric multigrid method improves the computational efficiency of such problems by providing more effective iteration updates [1,2] and reducing problem sizes [3] if multiscale adaptivity is introduced. Early multigrid methods mainly focused on spatial dimensions while Falgout et al. [4] recently extended such methods to include the time dimension. Examples of space-time multigrid methods involving adaptivity include elastodynamics [5], poroelasticity [6] and nonlinear multiphase flow in porous media [7].

Although providing substantial computational speedup, multigrid methods often suffer from high frequency residuals. After grid refinement, the prolongation process uses linear interpolation to provide an update for the unknowns on the finer mesh, which is insufficient for nonlinear problems with rough coefficients. The coarse solution used to produce the linear prolongation is acquired using upscaled coefficients calculated by numerical homogenization, which assumes the coefficient smoothness to be at least C^1. Consequently, such upscaling algorithm is inadequate to capture the complex structures of rough coefficients in the coarse resolution. An example is shown in Figure 1. Here a multiphase flow in porous media with channelized permeability coefficients is presented. The high contrast of permeability at the channel boundary causes the saturation solution to be discontinuous, leading to inaccurate linear interpolation. Here we observe high frequency residuals appearing sporadically but mostly along the channel boundary. As the Newton method resumes, the

CONTACT Hanyu Li lihanyu234@utexas.edu

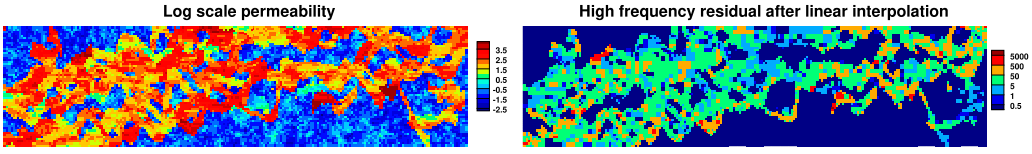

Figure 1. High frequency residual after linear interpolation of the multigrid method for rough coefficient cases.

first few iterations focus on reducing such high frequency residuals while little effort is devoted to the remaining system, resulting in suboptimal convergence behavior.

In this paper, we introduce a stable local residual minimization approach to enhance the prolongation process which provides an opportunity for improving the numerical homogenization. We use the multiphase flow in a porous media model for demonstration, while the idea is generally applicable to other time-dependent nonlinear problems. In Section 2, we present a model problem followed by a smoothing algorithm in Section 3. Results from numerical experiments using the proposed algorithm are discussed in Section 4. The summary of our findings follows in Section 5.

2. Flow model problem

We consider the following two-phase flow in the porous media model. The phase mass conservation, constitutive equations, boundary and initial conditions are as follows:

$$\frac{\partial(\phi\rho_\alpha s_\alpha)}{\partial t} + \nabla\cdot\boldsymbol{u}_\alpha = q_\alpha \quad \text{in } \Omega\times J, \tag{1}$$

$$\boldsymbol{u}_\alpha = -K\rho_\alpha\frac{k_{r\alpha}}{\mu_\alpha}(\nabla p_\alpha - \rho_\alpha \boldsymbol{g}) \quad \text{in } \Omega\times J, \tag{2}$$

$$\boldsymbol{u}_\alpha\cdot\boldsymbol{v} = 0 \quad \text{on } \partial\Omega\times J, \tag{3}$$

$$\begin{cases} p_\alpha = p_\alpha^0 \\ s_\alpha = s_\alpha^0 \end{cases} \quad \text{at } \Omega\times\{t=0\}, \tag{4}$$

for $\alpha = nw, w$. $J = (0, T]$ is the time domain of interest, while Ω is the spatial domain. Here, ϕ is porosity and K is permeability. ρ_α, s_α, $\boldsymbol{u}_\alpha$ and q_α are density, saturation, velocity and source/sink, respectively, for each phase. The phase densities are defined by Equation (5) for slightly compressible fluid

$$\rho_\alpha = \rho_{\alpha,ref}\cdot \mathrm{e}^{c_\alpha(p_\alpha - p_{\alpha,ref})}, \tag{5}$$

with c_α being the fluid compressibility and $\rho_{\alpha,ref}$ being the reference density at reference pressure $p_{\alpha,ref}$. In addition, $k_{r\alpha}$, μ_α and p_α are the relative permeability, viscosity and pressure for each phase. The relative permeability, often being the degenerate coefficient, is a function of saturation. Pressure differs between a wetting phase and non-wetting phase in the presence of capillary pressure, which is also a function of saturation:

$$k_{r\alpha} = f(s_\alpha), \tag{6}$$

$$p_c = g(s_\alpha) = p_{nw} - p_w. \tag{7}$$

The saturation of all phases obeys the following constraint:

$$\sum_\alpha s_\alpha = 1. \tag{8}$$

We now provide the weak variational form in space-time setting, which is also valid for traditional time-stepping schemes with uniform timesteps. We solve the system with a mixed finite

element method. Let $\boldsymbol{V} = H(\mathrm{div};\Omega)$, $W = L^2(\Omega)$ with $\boldsymbol{V}_h$ and W_h being their respective finite-dimensional subspaces. Let $J_n = (t_n, t_{n+1}]$ be the nth partition of the time domain of interest. Then for each space-time slab $J_n \times \Omega$, we define velocity and pressure/saturation spaces as, for any element $E_i = T_i \times F_i$,

$$\boldsymbol{V}_h^n = \left\{ \boldsymbol{v} \in L^2\left(J_n; H(\mathrm{div};\Omega)\right) : \boldsymbol{v}(\cdot,\boldsymbol{x})\big|_{F_i} \in \boldsymbol{V}_h, \boldsymbol{v}(t,\cdot)\big|_{T_i} = \sum_{a=1}^{l} \boldsymbol{v}_a t^a \ \&\ \boldsymbol{v}_a \in \boldsymbol{V}_h \right\},$$

$$W_h^n = \left\{ w \in L^2\left(J_n; L^2(\Omega)\right) : w(\cdot,\boldsymbol{x})\big|_{F_i} \in W_h, w(t,\cdot)\big|_{T_i} = \sum_{a=1}^{l} w_a t^a \ \&\ w_a \in W_h \right\}.$$

Functions in $\boldsymbol{V}_h^n$ and W_h^n along the time dimension are represented by polynomials with degrees up to l. We formulate the space-time variational formulation as follows: find $\boldsymbol{u}_{\alpha,h}^n \in \boldsymbol{V}_h^n$, $\tilde{\boldsymbol{u}}_{\alpha,h}^n \in \boldsymbol{V}_h^n$, $s_{\alpha,h}^n \in W_h^n$, $p_{\alpha,h}^n \in W_h^n$ such that

$$\int_{J_n}\int_{\Omega} \partial_t\left(\phi\rho_{\alpha,h}^n s_{\alpha,h}^n\right) w + \int_{J_n}\int_{\Omega}\left(\nabla\cdot\boldsymbol{u}_{up,\alpha,h}^n\right) w = \int_{J_n}\int_{\Omega} q_\alpha w \quad \forall\, w \in W_h^n, \tag{9}$$

$$\int_{J_n}\int_{\Omega} K^{-1}\tilde{\boldsymbol{u}}_{\alpha,h}^n \cdot \boldsymbol{v} = \int_{J_n}\int_{\Omega} p_{\alpha,h}^n \nabla\cdot\boldsymbol{v} \quad \forall\, \boldsymbol{v} \in \boldsymbol{V}_h^n, \tag{10}$$

$$\int_{J_n}\int_{\Omega} \boldsymbol{u}_{\alpha,h}^n \cdot \boldsymbol{v} = \int_{J_n}\int_{\Omega} \lambda_\alpha \tilde{\boldsymbol{u}}_{\alpha,h}^n \cdot \boldsymbol{v} \quad \forall\, \boldsymbol{v} \in \boldsymbol{V}_h^n. \tag{11}$$

The mobility ratio in λ_α is given as

$$\lambda_\alpha = \frac{k_{r\alpha}\rho_\alpha}{\mu_\alpha}, \tag{12}$$

and the upwind velocity is calculated by

$$\int_{J_n}\int_{\Omega} \boldsymbol{u}_{up,\alpha,h}^n \cdot \boldsymbol{v} = \int_{J_n}\int_{\Omega} \lambda_\alpha^* \tilde{\boldsymbol{u}}_{\alpha,h}^n \cdot \boldsymbol{v} \quad \forall\, \boldsymbol{v} \in \boldsymbol{V}_h^n. \tag{13}$$

The additional auxiliary phase fluxes $\tilde{\boldsymbol{u}}_{\alpha,h}^n$ are used to avoid inverting zero phase relative permeability [8]. λ_α^* denotes the upwind mobility ratio and its calculation is done by using saturations from the grid cell on the upwind direction of the pressure gradient.

3. Local residual minimization

Previous work regarding residual smoothing mainly involved linear problems with rough coefficients. In [9], an energy minimization method was introduced, which solves for a coarse basis function that minimizes the energy functional on the fine grid. However, the direct application of such an approach on nonlinear transport is problematic since no energy functional can be constructed due to the degenerate coefficients. Therefore, the local residual minimization approach is formulated.

Consider $\mathcal{T}_H^n$ as a coarse partition of $J_n \times \Omega$ with elements $E_{i,H}$ being refined into a finer partition $\mathcal{T}_h^n$ with elements $E_{j,h}$. We define the linear interpolation of any piecewise constant function (pressure

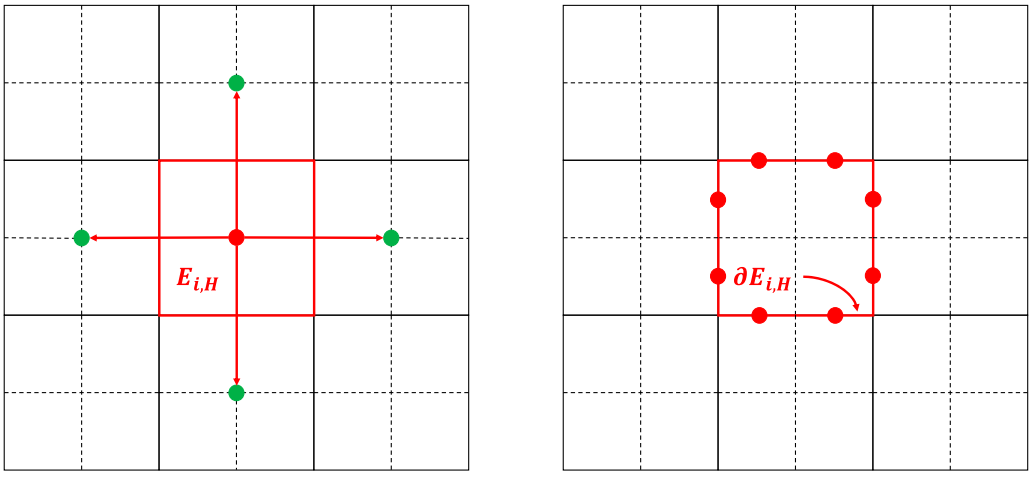

Figure 2. Four-point stencil on the coarse grid for boundary interpolation nodes (right plot).

and saturation) in space as f_ζ. Then the local problem is constructed as follow:

$$\int_{E_{i,H}} \left(\partial_t \left(\phi \rho^n_{\alpha,h} s^n_{\alpha,h} \right) + \nabla \cdot \boldsymbol{u}^n_{up,\alpha,h} - q_\alpha \right) w = 0 \quad \forall\, w \in W^n_h,\ \forall\, E_{i,H} = \bigcup_{E_{j,h} \subsetneq E_{i,H}} E_{j,h}, \tag{14}$$

subject to

$$\begin{cases} p_\alpha = p_{\alpha,\zeta} \\ s_\alpha = s_{\alpha,\zeta} \end{cases} \quad \text{on } \partial E_{i,H}. \tag{15}$$

Figure 2 demonstrates the two partitions and boundary interpolation nodes necessary to solve the local problem. If the interpolated pressure and saturation on the boundary are exact, then Equation (14) is well posed and provides a unique solution that matches the global solution on the local subdomain. However, providing exact boundary conditions by linear interpolation of the coarse solution is hardly achievable in nonlinear transport, and thus, the local problem tends to be ill-posed. Regarding the situation, we reformulate Equation (14) into a minimization problem as follows:

$$\min_{p_{\alpha,h}, s_{\alpha,h}} \left\{ \left\| \int_{E_{i,H}} \left(\partial_t \left(\phi \rho^n_{\alpha,h} s^n_{\alpha,h} \right) + \nabla \cdot \boldsymbol{u}^n_{up,\alpha,h} - q_\alpha \right) w \right\|_\infty \right\} \quad \forall\, w \in W^n_h,\ \forall\, E_{i,H} = \bigcup_{E_{j,h} \subsetneq E_{i,H}} E_{j,h}. \tag{16}$$

Similar to solving the global problem, we use Newton's method for such optimization process. Note that the residual functional for a nonlinear transport equation is non-convex. Therefore, to prevent over-working the local problem and cause divergence issues on the global solution process afterwards, the iteration is stopped once reaching the average background residual instead of the absolute minimum.

Previous work [10] has shown promising results that the local residual minimization approach is effective, even for complex models, in reducing high frequency residuals caused by inadequate saturation interpolation. However, such an approach is suboptimal for regions with complex channel structures. Due to the limited number of coefficients in the subdomain, the local problem cannot determine a definite flow path, resulting in limited improvement on the initial guess, or even optimization failure for more complicated models.

Oversampling techniques have been widely applied in numerical homogenization [11] to upscale channelized permeability while maintaining proper inter-cell connectivity. We enhance this approach

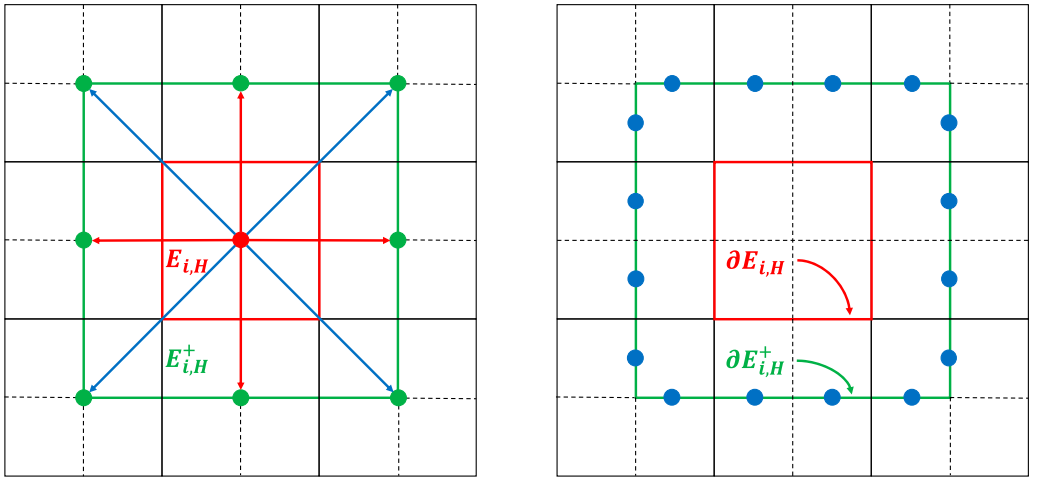

Figure 3. Nine-point stencil on the coarse grid for extended boundary interpolation nodes (right plot).

to local residual minimization as demonstrated in Figure 3. Here, the local problem has been extended from $E_{i,H}$ to $E^+_{i,H}$ by an extra layer of fine elements. To accurately interpolate nodes on the extended boundary, a 9-point stencil including diagonal direction gradients is necessary. Although increasing the size of the local problem, this extra layer is essential for forming a definite flow path, which facilitates optimization and prevents failure.

4. Numerical results

We use the space-time geometric multigrid algorithm introduced in [7] to solve the described system. The procedure starts by solving the global problem at its coarsest resolution in the space-time domain and then sequentially refines certain regions to its finest resolution. The coarsest time step is chosen such that the numerical convergence is guaranteed on the coarsest spatial grid. During the sequential refinement process, the solver first keeps the spatial mesh static at its coarsest level and searches for regions to refine in time. Once the last level of temporal refinement is implemented, the temporal discretization is finalized and the solver refines the mesh in space until reaching the finest resolution. Afterward, the grid is restored to the coarsest resolution, the solver marches forward in time with the coarsest time step and the whole process reiterates. The complete algorithm is illustrated in Figure 4. As shown in the flowchart, the local residual minimization step follows local mesh refinement and initial guess interpolation.

We apply the SPE10 dataset [12] bottom layer to conduct our numerical experiments. Figure 5 demonstrates the petrophysical properties. The fine-scale dimension is 56×216 elements of size 1 ft $\times$ 1 ft $\times$ 1 ft. The coarsest and finest timestep size is 10 and 1.25 days, respectively. The simulation continues for 600 days (water breakthrough). There are three levels of the coarse spatial grid with a refinement ratio of 2 between them. The coarse scale properties are calculated by numerical homogenization introduced in [13]. For nonlinear advection, we use the Brooks–Corey model illustrated in Figure 6 for both relative permeability and capillary pressure, which is described by

$$\begin{cases} k_{rw} = k^0_{rw}\left(\dfrac{s_w - s_{wirr}}{1 - s_{or} - s_{wirr}}\right)^{n_w}, \\ k_{ro} = k^0_{ro}\left(\dfrac{s_o - s_{or}}{1 - s_{or} - s_{wirr}}\right)^{n_o}, \end{cases} \tag{17}$$

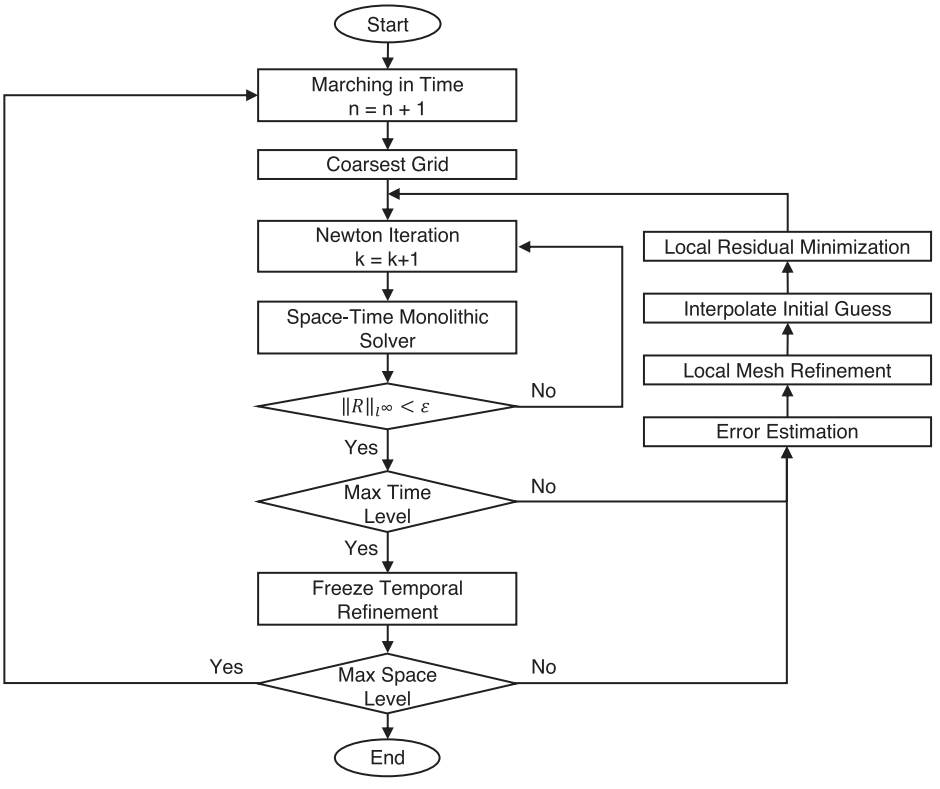

Figure 4. Solution algorithm for sequential local mesh refinement solver with separate temporal and spatial adaptivity.

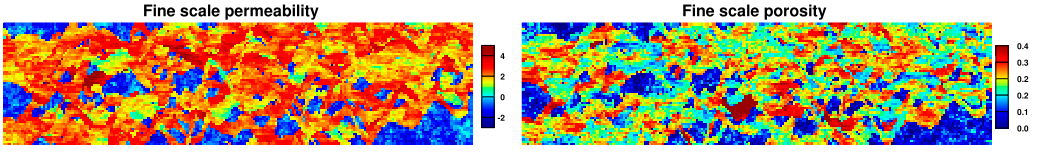

Figure 5. Fine-scale permeability and porosity of the numerical experiment.

$$p_c(s_w) = P_{en,cow}\left(\frac{1 - s_{wirr}}{s_w - s_{wirr}}\right)^{l_{cow}}. \tag{18}$$

The model parameter values are $s_{or} = s_{wirr} = 0.2$, $k^0_{ro} = k^0_{rw} = 1.0$, $n_w = n_o = 2$, $P_{en,cow} = 10$ psi and $l_{cow} = 0.2$. The fluid data are listed in Table 1. We place a water injection well with a rate of 1 ft^3/day at the bottom left corner and a production well with the production pressure of 1000 psi at the upper right corner. The initial pressure and saturation are set to be 1000 psi and 0.2, respectively.

We first present two snapshots generated during the simulation. As demonstrated in Figure 7, the difference between the saturation initial guess and true solution is quantified. For initial guess provided by direct linear interpolation (top plots), we observe a significant mismatch along the channel boundary and around low permeability spots inside the main channel. The notable variation of permeability in such regions causes the saturation solution to be discontinuous, a behavior that is not perceivable by linear interpolation. We then apply local residual minimization without oversampling (middle plots) and as illustrated, the over-estimation of saturation in low permeability regions is eliminated. However, there is still a noticeable mismatch, mainly in regions with complex channel

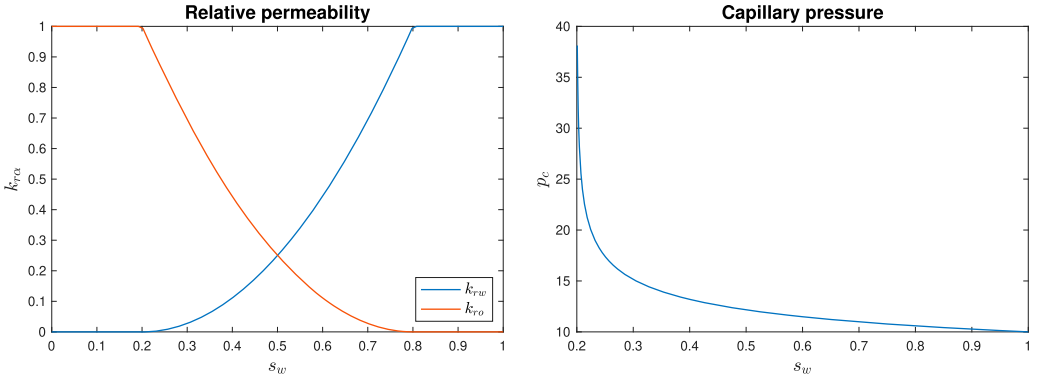

Figure 6. Relative permeability (left) and capillary pressure (right) curve for the numerical experiment.

Table 1. Fluid data for the numerical experiment.

Parameter	Value	Unit
Oil compressibility (c_o)	1.0×10^{-4}	psi^{-1}
Water compressibility (c_w)	3.0×10^{-6}	psi^{-1}
Oil viscosity (μ_o)	3.0	cp
Water viscosity (μ_w)	1.0	cp
Oil standard density ($\rho_{o,std}$)	53	lb/ft^3
Water standard density ($\rho_{w,std}$)	64	lb/ft^3

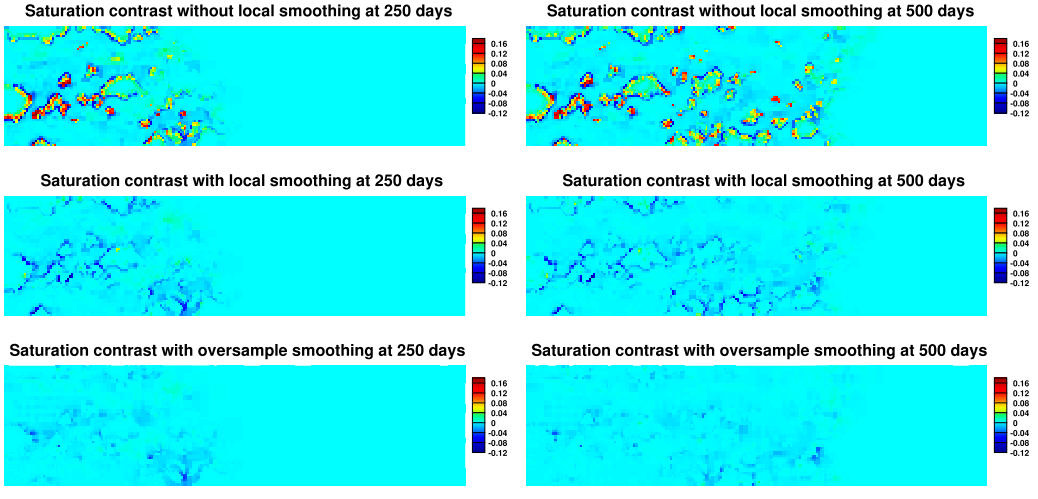

Figure 7. Saturation contrast between initial guess and true solution without local smoothing (top), with local smoothing (middle) and with oversample local smoothing (bottom).

structures such as sharp corners and thin conduits. The results with oversampling (bottom plots) show significant improvement. The complex structures possess less obstacles to the optimization process. Therefore, most of the mismatch has been removed.

We now compare the computational behavior of the two local minimization methods. Figure 8 demonstrates the optimization iteration taken in each timestep and the cumulative CPU time to finish all the local problems. The iteration number increases for both methods during early timesteps, due to the expanding saturation front which results in more refinement subdomains. With additional

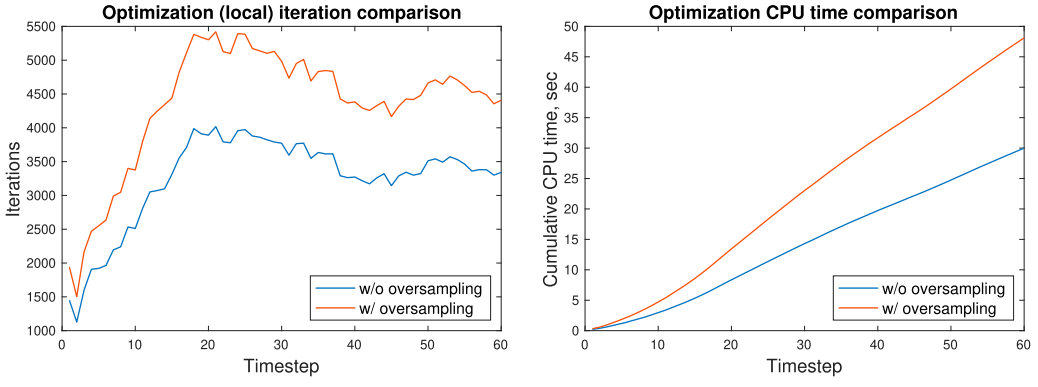

Figure 8. Stepwise iteration count and cumulative CPU time for a local residual minimization problem.

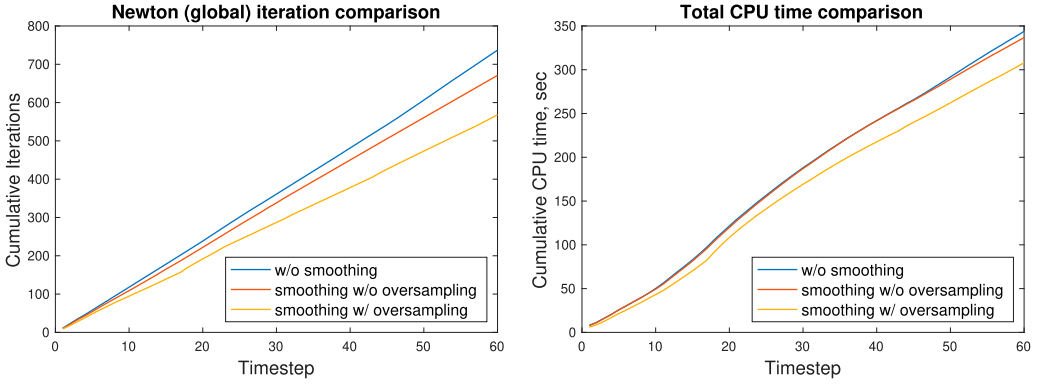

Figure 9. Cumulative iteration count and CPU time for a global problem.

data provided by oversampling, the local system gains more constraints during the optimization. Consequently, such an approach requires more iterations than the local problem without oversampling. Also due to the increased problem sizes, the total CPU time to solve the oversampled problems is increased by approximately 50%.

Regarding the computational behavior of the global problem, Figure 9 illustrates the cumulative global iterations and the total CPU time to finish the simulation. Note that such cumulative time also includes those spent on local residual minimization. We observe that the smoothing without oversampling provides a slight improvement on the Newton convergence of the global problem. However, such improvement is not substantial enough to counteract the additional time spent on local smoothing. Consequently, there is very limited speedup on the total simulation time. On the other hand, the local residual minimization with oversampling reduces the global iteration by approximately 25%. Therefore, despite the increased computational load on the local problem, such approach still provides a 15% speedup on the total computing time.

5. Conclusions

In this paper, we present a stable local residual minimization algorithm for the geometric multigrid method to remove high frequency residuals caused by the prolongation step. The minimization is achieved by solving the global system restricted to each refinement subdomain with boundary conditions provided by linear interpolation of the coarse solution. The local problem is solved in the sense of optimization by Newton's method and the iteration is terminated once reaching the background

residual, to prevent over-working the ill-posed local problem. To improve algorithm stability and minimization outcome, oversampling is applied by adding an extra layer of fine elements to the original subdomain. Results from the numerical experiment using the two-phase slightly compressible flow model with rough coefficients are presented. We observe that the local smoothing with oversampling erased the majority of the difference between the saturation initial guess and true solution, regardless of coefficient structure complexity. The number of global iterations required for convergence is reduced by 25% and the total CPU time is diminished by 15%. Considering the slightly compressible immiscible system is fairly stable and the adaptive method already providing tremendous computational speedup, there is naturally not much room for improving the computational efficiency. However, based on the result, we do expect local residual minimization to be majorly beneficial towards more complicated and chaotic systems, where an inadequate initial guess can easily lead to convergence failure. And also towards uniformly high-resolution simulations, where multigrid refinement occurs globally. Preliminary results indicate that oversampling is particularly advantageous to local problems on complex models that include compressible phase, such as the black-oil model, to prevent optimization failure.

Disclosure statement

No potential conflict of interest was reported by the author(s).

References

[1] Bank R, Dupond T, Yserentant H. The hierarchical basis multigrid method. Numer Math. 1988;52:427–458.
[2] Ghia U, Ghia K, Shin C. High-re solution for incompressible flow using the Navier-Stokes equations and a multigrid method. J Comput Phys. 1982;48:387–411.
[3] Amanbek Y, Singh G, Wheeler M, et al. Adaptive numerical homogenization for upscaling single phase flow and transport. J Comput Phys. 2019;387:117–133.
[4] Falgout R, Friedhoff S, Kolev TV, et al. Parallel time integration with multigrid. SIAM J Sci Comput. 2014;36:C635–C661.
[5] Hughes T, Hulbert G. Space-time finite element methods for elastodynamics: formulations and error estimates. Comput Methods Appl Mech Eng. 1988;66:339–363.
[6] Bause M, Radu F, Köcher U. Space-time finite element approximation of the Biot poroelasticity system with iterative coupling. Comput Methods Appl Mech Eng. 2017;320:745–768.
[7] Li H, Leung W, Wheeler M. Sequential local mesh refinement solver with separate temporal and spatial adaptivity for non-linear two-phase flow problems. J Comput Phys. 2020;403:Article 109074.
[8] Peszyńska M, Wheeler M, Yotov I. Mortar upscaling for multiphase flow in porous media. Comput Geosci. 2006;6:73–100.
[9] Wan WL, Chan TF, Smith B. An energy-minimizing interpolation for robust multigrid methods. SIAM J Sci Comput. 1998;21:1632–1649.
[10] Li H, Wheeler M. Local residual minimization smoothing for improving convergence behavior of space-time domain decomposition method. In: 26th Domain Decomposition Conference Proceedings; 2021. Accepted.
[11] Chung E, Efendiev Y, Hou T. Adaptive multiscale model reduction with generalized multiscale finite element methods. J Comput Phys. 2016;320:69–95.
[12] Christie M, Blunt M. Tenth SPE comparative solution project: a comparison of upscaling techniques. SPE Reserv Eval Eng. 2001;4:308–317.
[13] Efendiev Y, Hou T. Multiscale finite element methods: theory and applications. Vol. 4. New York, NY: Springer Science and Business Media; 2009.